Competing magnetic anisotropies in the magnetic and magnetoelastic properties of holmium-thulium superlattices

C. de la Fuente, J. I. Arnaudas, L. Benito, M. Ciria, and A. del Moral
Departamento de Magnetismo de Sólidos, Departamento de Física de la Materia Condensada and Instituto de Ciencia de Materiales de Aragón, Universidad de Zaragoza and CSIC, 50071, Zaragoza, Spain

R. C. C. Ward and M. R. Wells
Clarendon Laboratory, Park Road, OX1 3PU, Oxford, United Kingdom

(Received 18 October 2000; revised manuscript received 19 March 2001; published 14 August 2001)

We report on magnetic and magnetoelastic (MEL) stress measurements applying the magnetic field within the hexagonal basal plane of the Ho_8/Tm_{16} and Ho_{30}/Tm_{16} superlattices (SL's). To carry out the analysis of the results obtained for Ho/Tm SL's, we have compared them with the corresponding ones for Ho/Lu SL's. We have measured the zero-field-cooled dc susceptibility and the magnetization applying the magnetic field up to 12 T along the *b* axis and between 10 and 120 K. The zero-field-cooled susceptibility shows the coexistence of holmium and thulium magnetic orders below 58 K. The magnetization at high field shows that the magnetic moments of holmium ions are fully aligned along the field direction for $H>5$ T in Ho/Tm SL's, and that at the maximum field the thermal variation of magnetization of the thulium layers for Ho_8/Tm_{16} SL behaves very close to that of the bulk. In the Ho_{30}/Tm_{16} SL case, the low-temperature values of the magnetization indicate a larger in-plane magnetic moment of Tm, as compared to the Ho_8/Tm_{16} SL. The study of the effective basal-plane cylindrical symmetry-breaking MEL stress is clearly consistent with the magnetization results. The Tm layers behavior can be associated with a combination of a mean field, due to the Ho layers, and to a reduction of the axial anisotropy of Tm, due to the basal-plane cylindrical symmetry-breaking magnetoelastic strain in Tm blocks.

DOI: 10.1103/PhysRevB.64.094424 PACS number(s): 75.70.−i, 75.80.+q

I. INTRODUCTION

The magnetic properties of the thulium and holmium ions are dominated by their magnetocrystalline anisotropy. The axial anisotropy of thulium is very strong and much more intense than the basal-plane anisotropy of holmium.[1–4] Bulk holmium is ordered below $T_N=132$ K and changes its magnetic structure from in-plane helix to cone structure below $T_c=20$ K, having in this last structure a small ferromagnetic component along the *c* axis ($\simeq 10°$ out of the basal plane). The magnetoelastic (MEL) stress in the basal-plane of holmium hcp structure, $B^{\gamma,2}\cong+0.3$ GPa at 0 K, is not very strong compared with other rare-earth metals like Dy and Tb, however, it is enough to reduce the magnetocrystalline anisotropy energy and then favors the competition between the anisotropy, exchange, and the Zeeman energies. Due to that, the magnetic structures of holmium become very complex when a magnetic field is applied along the basal plane: distorted helix, helifan, fan, and ferromagnetic structures.[3–5] In these phases, the field necessary to obtain a completely saturated magnetization, $\simeq 3050$ emu/cm^3 at 0 K, is inferior to 5 T for $T<T_N$.[3–5] On the contrary, the bulk thulium has its magnetic structure longitudinally modulated along the *c* axis below $T_N=58$ K,[1,2] where the magnetic moments, first, order in a sinusoidal structure of wave vector $0.273c^*$ and then form below $T_{AF}=30$ K a square modulated antiphase structure of 4-3 type, of larger wave vector $2/7c^*$.[1,2] Its strong axial anisotropy hardly allows the magnetic moments to be tilted out of the *c* axis when a magnetic field is applied perpendicularly within the basal plane. This deviation is less than 2% of the total moment at low temperatures and high fields, $\simeq 10$ T.[6] However, a magnetic field applied parallel to the *c* axis can break the modulated structure along this axis, giving rise to a fully aligned magnetization state, $\simeq 2700$ emu/cm^3 at 0 K, for magnetic fields higher than 2.8 T.[6]

In the last years, the development of the epitaxial techniques has allowed the growth of rare-earth (RE) superlattices (SL's). As a part of the systematic studies on the magnetic properties and MEL stresses in RE SL's,[7–11] we have performed a *comparative* study of these properties in some holmium-thulium and holmium-lutetium SL's. In both kinds of SL's, the magnetic structures of holmium and thulium layers are similar (not the same) to those of the bulk holmium and thulium metals.[12,13] In holmium-lutetium SL's, the zero-field structures of holmium are clearly coherent through several bilayers.[12] On the other hand, in holmium-thulium SL's the zero-field magnetic structures in holmium and thulium layers show a degree of coherence across the bilayer lower than that in the holmium-lutetium case.[13] But, in both cases, an applied magnetic field should reduce the coherence of the magnetic structures, as it was observed in holmium-yttrium SL's.[23]

In this paper, we report on the study of several magnetic and MEL properties, which occur when a magnetic field is applied along the basal plane in the holmium-thulium and the holmium-lutetium SL's. We have chosen holmium-thulium SL's to study the effect of competing anisotropies in the magnetic and MEL behavior of layered structures. In previous works, we have studied the holmium-lutetium SL's;[8–10] here we shall present additional results on those SL's, taking

them as a well-known reference to analyze the holmium-thulium systems (in both cases, the holmium blocks are under compressive stress by the Tm or Lu layers). The analysis of the magnetization curves will allow us to propose magnetic-phase diagrams (MPD) for the studied SL's. The magnetic phases were identified by comparing our results with the measurements that have been obtained by using the neutron-diffraction technique for bulk holmium and thulium,[1–4] and for Ho/Lu and Ho/Tm SL's.[12,13] In the holmium-thulium SL's case, the magnetization could also give valuable information about the magnetic interaction existing between the holmium and thulium layers. Moreover, due to the single-ion character of the MEL coupling associated with the basal-plane cylindrical symmetry breaking,[14,15] the MEL stress measurements presented in this work could help us to investigate the competition between the anisotropies of holmium and thulium ions, mediated by the interlayer Ho/Tm exchange coupling.

II. SUPERLATTICES AND MAGNETIC AND MAGNETOELASTIC MEASUREMENTS

The SL's studied in this work have been grown by molecular-beam epitaxy in the LaMBE facility at the Clarendon Laboratory (Oxford). The growth process was similar to that described by Ward *et al.*[16] The substrate is a single crystal of sapphire, upon which is deposited a thin film (buffer) of niobium. This prevents the reaction of rare-earth elements, which are highly reactive with the substrate. A seed of yttrium was used, which has a similar hcp structure to the Ho/Lu and Ho/Tm SL's. After growing the SL structure, a cap of yttrium was used to isolate the rare-earth layers from the air. During the growth process the substrate temperature and the deposition rates were chosen to allow the samples to be grown epitaxially with the desired structure. The SL structure was investigated *in situ* by reflection high-energy electron diffraction and *ex situ* by x-ray diffraction. The crystalline-coherence length of the SL's studied is about 2000 Å. Their mosaic spread is typically 0.4°, and the average interdiffusion at the interfaces is estimated from x-ray diffraction as two atomic planes.[13,17] Nominally the samples were Ho_8/Tm_{16} and Ho_{30}/Tm_{16}, where the subscripts refer to the number of atomic planes of each element within the bilayer repeat, which was 60 times. The low-field susceptibility measurements, zero-field cooled (ZFC), were performed by using a superconducting quantum interference device magnetometer with the magnetic field applied along the *b*-axis direction, in order to probe the magnetic phases existing at nearly zero field. The measurements of magnetization at high field were done with a vibrating-sample magnetometer (VSM) magnetometer, applying also the magnetic field parallel to the basal plane (*b* axis), for temperatures between 10 and 110 K and up to 12 T.

The MEL-stress measurements were carried out by using a capacitive cantilever technique. The measurement process was similar to the one described by Ciria *et al.*[7,11] The samples have a rectangular shape, with the edges parallel to the *b* axis and *a* axis, respectively, having a typical size of $\cong 6 \times \cong 8$ mm^2. In our experimental setup of the capacitive cell, the sample is clamped along an α direction, which can be parallel to either of its edges, and the metallic part of the sample acts as one side of the capacitor. The other electrode is a copper deposit sputtered onto a plate of fused quartz, which guarantees a good behavior under thermal cycling. The sapphire substrate was thinned down to ~ 150 μm to increase the sensitivity of the method. Under the MEL stresses developed in the SL, the substrate is bent, and this bending produces capacitance changes, which we measure with a capacitance bridge Andeen-Hagerling model 2500 A, with a nominal sensitivity of 0.5 aF. The capacitive cell was placed in a helium continuous flow cryostat mounted inside of a superconducting cryomagnet, which allows us to measure at temperatures between 1.7 and 300 K. The magnetic field is applied along a β direction, which, in our case, will be held parallel to the *b* axis, 12 T being the maximum field applied. Each isotherm was obtained after demagnetizing the samples by heating up first above the Néel temperature of Ho blocks and then cooling down to the desired temperature. Assuming a small deflection, it can be shown[7,11] that the cantilever deflection produces a capacitance variation,

$$\Delta C_{(\beta,\alpha)} = -\frac{C^2_{0(\beta,\alpha)} L^2_{(\beta,\alpha)}}{6\varepsilon_0 A_{(\beta,\alpha)}} \cdot \frac{1}{R_\alpha}, \tag{2.1}$$

where $C_{0(\alpha,\beta)}$ is the initial capacitance at zero field, $A_{(\beta,\alpha)}$ and $L_{(\beta,\alpha)}$ are the area and the length of the plate, respectively, ε_0 is the vacuum dielectric constant, and $1/R_\alpha$ is the curvature of the plate. As an example, if we consider the typical values of $L_{(\beta,\alpha)} \simeq 8$ mm, $A_{(\beta,\alpha)} \simeq 48$ mm^2, and $C_{0(\beta,\alpha)} = 3.34$ pF, then the minimum-capacitance variation (10^{-6} pF) corresponds to a curvature radius of the plate R_α of around 10^6 m.

III. EXPERIMENTAL RESULTS

A. ZFC susceptibility and magnetization measurements

The magnetization of SL's has been measured with the magnetic field applied along the hexagonal basal plane (hcp) of the SL structure. In Figs. 1(a)–1(d) we plot the zero-field-cooled susceptibility (ZFC), which has been measured at 5×10^{-3} T, applying the magnetic field along the *b* axis, ($\vec{\mathbf{b}} = [010]$ direction), for both Ho/Lu and Ho/Tm SL's. In the Ho/Lu SL's [see Figs. 1(a) and 1(b)] the Néel temperature T_N is $\simeq 130$ K for Ho_{30}/Lu_{15} and $\simeq 115$ K for Ho_8/Lu_{15}, and below this ordering temperature the ZFC susceptibility increases when the temperature decreases. This increment is monotonous reaching a maximum at $\simeq 30$ K for Ho_{30}/Lu_{15} and $\simeq 53$ K for Ho_8/Lu_{15}. Afterward, due to the diamagnetic effect of the superconducting niobium buffer the susceptibility quickly decreases to negative values, especially below $T_{SC} \cong 10$ K, which is the niobium superconducting temperature. For the Ho/Tm SL's, the Néel temperatures of holmium and thulium layers can be observed *separately* [see Figs. 1(c) and 1(d)]. For the Ho_{30}/Tm_{16} SL, the Néel temperature of holmium layers is $\simeq 130$ K, slightly smaller than the bulk's value, whereas for the Ho_8/Tm_{16} SL is $\simeq 105$ K, which is quite far from the bulk holmium one [the reduction of T_N(Ho) correlates with the ''dilution'' of the systems]. In

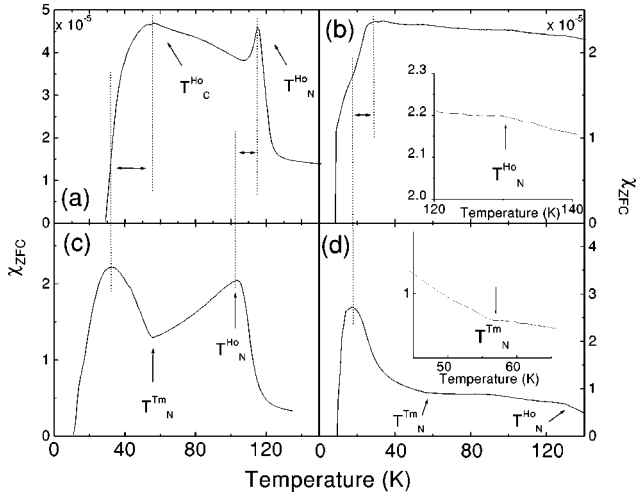

FIG. 1. Zero-field-cooled dc susceptibility at 5 mT for (a) Ho_8/Lu_{15}, (b) Ho_{30}/Lu_{15}, (c) Ho_8/Tm_{16}, and (d) Ho_{30}/Tm_{16} superlattices. The arrows indicate the magnetic transition temperatures of holmium and thulium layers. The dotted lines separate the different magnetic phases for (a) Ho_8/Lu_{15} and (c) Ho_8/Tm_{16} (notice the shift between the dotted lines). The inset plots for (b) Ho_{30}/Tm_{16} and (d) Ho_{30}/Tm_{16} indicate more accurately the Néel temperatures of holmium blocks at the ZFC susceptibility.

the Ho_{30}/Tm_{16} [Fig. 1(d)] there exists a small inflection around 90 K, which is followed by a flat region down to 60 K, where the susceptibility hardly changes. However, in the Ho_8/Tm_{16} case, the ZFC susceptibility suffers an important decrease below T_N(Ho) [see Fig. 1(c)], which changes drastically in its slope for temperatures below 58 K.

In Figs. 2(a)–2(d), we show magnetization isotherms between 10 and 120 K and at a maximum applied field of 12 T. In the Ho/Lu SL's [see Figs. 2(a) and 2(b)] the magnetization M curves are similar at low temperatures for both samples, being saturated at $\simeq 950$ emu/cm^3 for Ho_8/Lu_{15} and $\simeq 2000$ emu/cm^3 for Ho_{30}/Lu_{15}, when the applied magnetic

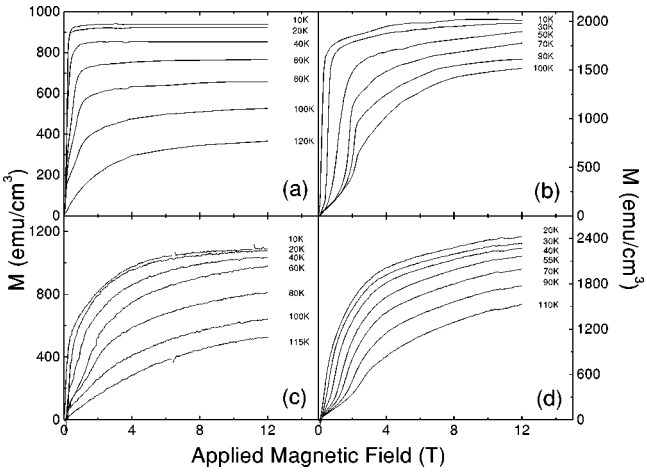

FIG. 2. Magnetization isotherms M for (a) Ho_8/Lu_{15}, (b) Ho_{30}/Lu_{15}, (c) Ho_8/Tm_{16}, (d) Ho_{30}/Tm_{16} superlattices. The magnetization units (emu/cm^3) were obtained by estimating the total volume of the superlattice.

field is above $\gtrsim 0.5$ T (notice that M values of Fig. 2 are written in emu per cubic centimeter of the SL volume) and the temperature is $\simeq 10$ K. These values indicate that the low-temperature magnetization isotherms are very close to the total expected saturation, using the *bulk* values, i.e., $\simeq 1000$ emu/cm^3 for Ho_8/Lu_{15} and $\simeq 2050$ emu/cm^3 for Ho_{30}/Lu_{15}. Opposite to what happens with the Ho/Lu SL's, the magnetization isotherms of the Ho/Tm SL's are *not* saturated at all, although the magnetization curves of the Tm-rich Ho_8/Tm_{16} seem to be more saturated than in the Ho-rich case, Ho_{30}/Tm_{16} [see Figs. 2(c) and 2(d)]. The magnetization curves get values close to $\simeq 1100$ emu/cm^3 for Ho_8/Tm_{16} and $\simeq 2500$ emu/cm^3 for Ho_{30}/Tm_{16} for low temperatures and at the maximum field applied. In this case, the magnetization values are *far* from the total saturation, because the total magnetization expected at a full saturation regimen and low temperatures is around 2800 emu/cm^3 for Ho_8/Tm_{16} and $\simeq 2950$ emu/cm^3 for Ho_{30}/Tm_{16}, by using the bulk values. The magnetization reduction for Ho_8/Tm_{16} SL is quite remarkable.

B. Magnetoelastic stress measurements

1. Experimental results

We shall define the MEL stress $\sigma(\beta,\alpha)$ as the one associated with the bending of the bimorph "superlattice-sapphire substrate," when the magnetic field is applied along the β direction and the clamping of the samples is along the α direction. In our case, β is $\vec{\mathbf{b}}=[010]$ and α can be $\vec{\mathbf{b}}=[010]$ or $\vec{\mathbf{a}}=[100]$; $\vec{\mathbf{a}}$ and $\vec{\mathbf{b}}$ are directions within the growing plane of the samples. The MEL stress produces a curvature of the plate, $1/R_\alpha$, in the plane perpendicular to α. The curvature is related to the capacitive variations $\Delta C_{(\beta,\alpha)}$, measured with our cantilever capacitive technique, through Eq. (2.1). In the next section, we shall establish the relation between the curvature of the plate and the MEL stress $\sigma(\beta,\alpha)$. But for now, we shall briefly make some comments about the MEL stress isotherms. The $\sigma(\beta,\alpha)$ isotherms are plotted in Figs. 3 and 4, for temperatures between 10 and 120 K and applied magnetic field up to 12 T (temperatures below or close to 10 K were avoided because of the proximity of the diamagnetic behavior of the superconducting niobium buffer). In Figs. 3 and 4 we show the $\sigma([010],[010])$ and $\sigma([010],[100])$ MEL stress isotherms for Ho/Lu and Ho/Tm SL's, respectively. The MEL stress isotherms for Ho/Lu SL's are quite similar in their shape to the magnetization ones, reaching a saturation regime at relatively small magnetic fields, $H>0.5$ T, and becoming more saturated when decreasing the temperature.

In Figs. 4(a)–4(d) are presented the MEL stress isotherms for the Ho/Tm SL's. Their field dependencies are quite complex. They also are, in general, fully different with respect to those in Ho/Lu SL's, especially for the $\sigma([010],[010])$ MEL stresses. The $\sigma([010],[100])$ MEL stresses for Ho_{30}/Tm_{16} are, to some extent, similar in shape to the corresponding ones of Ho_{30}/Lu_{15} [see Fig. 3(d)], although their values are smaller, and show a strong change in their field variation for temperatures below T_N(Tm)$\simeq 58$ K [see Fig. 4(b)]. These

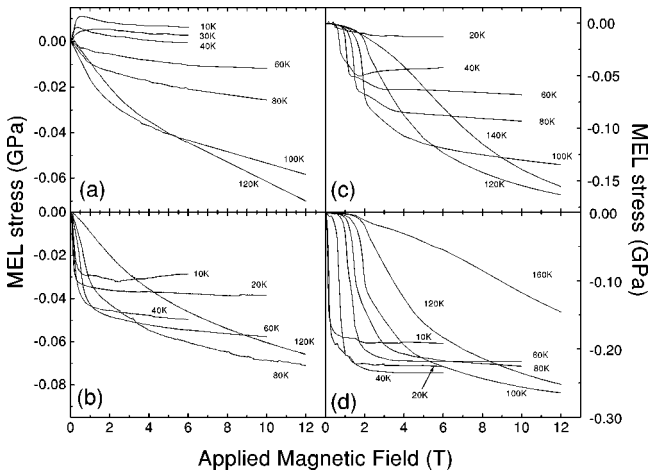

FIG. 3. Magnetoelastic stress isotherms parallel: (a) and (c) $\sigma([010],[010])$, and perpendicular: (b) and (d) $\sigma([010],[100])$, to the [010] direction applied magnetic field for (a) and (b) Ho_8/Lu_{15}, and for (c) and (d) Ho_{30}/Lu_{15} superlattices.

inflections in the field dependence are clearly related to the appearance of magnetic order in the thulium layers along the easy $\vec{\mathbf{c}}$ axis at $T_N(\mathrm{Tm}) \simeq 58$ K.

2. Basal-plane cylindrical symmetry breaking (CSB) magnetoelastic stress

We have used the theory of pure bending of plates[18] to correlate the MEL stress in the plate $\sigma(\beta,\alpha)$ with its curvature $1/R_\alpha$ in the way we have done in our previous MEL studies of HCP rare-earth SL's.[8,11] In the following, the notation of the SL samples is $[A_{t_A}/B_{t_B}]_N$, where t_A and t_B are the thickness of the "*A*" and "*B*" layers, respectively; *N* is the number of bilayers and $A=$Ho and $B=$Lu or Tm. We have assumed that, in a first-order approximation, the symmetry MEL energy density for our rare-earth SL is quadratic in the spin components and linear in the strains. Then, the MEL plus elastic free-energy densities for the *A* and *B* layers,

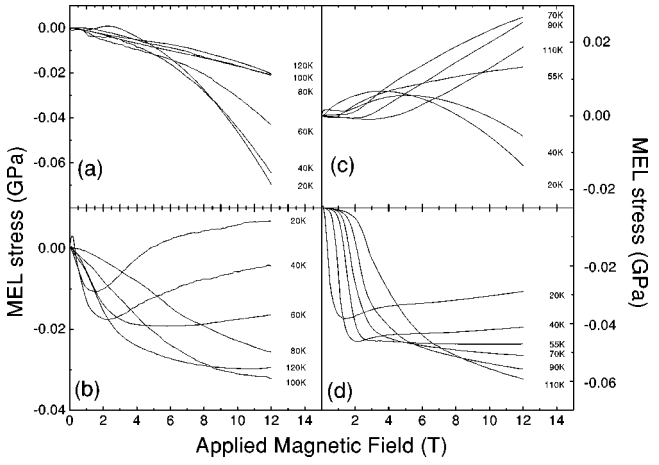

FIG. 4. Magnetoelastic stress isotherms parallel: (a) and (c) $\sigma([010],[010])$, and perpendicular: (b) and (d) $\sigma([010],[100])$, to the [010] direction applied magnetic field, (a) and (b) for Ho_8/Tm_{16}, and (c) and (d) for Ho_{30}/Tm_{16} superlattices.

$e_{MEL+EL}(i)$ $(i=A,B)$, are written taking into account the hexagonal symmetry of the rare-earth layers,[14] and for simplicity restricting only to the relevant $\epsilon_1^\gamma=(\epsilon_{xx}-\epsilon_{yy})/2$ strain, breaking the basal-plane cylindrical symmetry,

$$e_{MEL+EL}(i) = -\frac{1}{2}B^{\gamma,2}(i)\epsilon_1^\gamma(i)[\alpha_x^2(i)-\alpha_y^2(i)] + \frac{1}{2}c^\gamma(i)\epsilon_1^\gamma(i)^2+\cdots. \tag{3.1}$$

In Eq. (3.1), $\alpha_x(i)$ and $\alpha_y(i)$ are the direction cosines of the magnetization, $\mathbf{M}(i)$, for the *i* layers; $B^{\gamma,2}(i)$ is the CSB MEL stress, which gives rise to the $\epsilon_1^\gamma=(\epsilon_{xx}-\epsilon_{yy})/2$ magnetostrictive strain and $c^\gamma(i)$ is the γ-mode symmetry elastic stiffness constant.

After the minimization (imposing the boundary conditions for the plate bending) of the total energy E_{Tot} contributed by the elastic energy of the substrate[8,11] plus the elastic and MEL energies of the whole SL, we get the equilibrium curvature radius as a function of the MEL stress of the *i* layers. In this procedure, we have assumed that the clamping of our flat samples imposes that the curvature is only important in a plane, which is perpendicular to the clamping line. We also assume that, under an applied magnetic field along $\vec{\mathbf{b}}=[010]$, the magnetic moments of the holmium layer is aligned along [010], and for the thulium layer, the magnetic moments are tilted out of the $z\|[001]$ direction, following a certain angle distribution γ, which is *z* dependent. Then, we can get the following equilibrium equations:

$$\frac{\partial E_{Tot.}(\mathbf{H}\|[010])}{\partial R_x^{-1}} = \frac{2}{3}\sigma([010],[010]) + \frac{t_{\mathrm{Ho}}}{t_{\mathrm{Ho}}+t_{\mathrm{Tm}}}\left(\frac{1}{6}B^{\gamma,2}(\mathrm{Ho})\mathcal{B}_1(\mathrm{Ho})\right) + \frac{t_{\mathrm{Tm}}}{t_{\mathrm{Ho}}+t_{\mathrm{Tm}}}\left(\frac{1}{6}B^{\gamma,2}(\mathrm{Tm})\langle\sin^2\gamma\rangle + \mathcal{B}_2(\mathrm{Tm})\right)=0, \tag{3.2}$$

$$\frac{\partial E_{Tot.}(\mathbf{H}\|[010])}{\partial R_y^{-1}} = \frac{2}{3}\sigma([010],[100]) - \frac{t_{\mathrm{Ho}}}{t_{\mathrm{Ho}}+t_{\mathrm{Tm}}}\left(\frac{1}{6}B^{\gamma,2}(\mathrm{Ho})-\mathcal{B}_1(\mathrm{Ho})\right) - \frac{t_{\mathrm{Tm}}}{t_{\mathrm{Ho}}+t_{\mathrm{Tm}}}\left(\frac{1}{6}B^{\gamma,2}(\mathrm{Tm})\langle\sin^2\gamma\rangle - \mathcal{B}_2(\mathrm{Tm})\right)=0, \tag{3.3}$$

where $\langle\cdots\rangle$ is a volume average over the angular distribution $\gamma(z)$ of Tm moments out of the *c* axis. The $\sigma(\beta,\alpha)$ MEL stresses in Eqs. (3.2) and (3.3) are given by

$$\sigma([010],[010]) = \frac{1}{6}\frac{h_{subs}^2}{N(t_{\mathrm{Ho}}+t_{\mathrm{Tm}})}\left(\frac{C_{xx}}{R_x}\right), \qquad (3.4)$$

$$\sigma([010],[100]) = \frac{1}{6}\frac{h_{subs}^2}{N(t_{\mathrm{Ho}}+t_{\mathrm{Tm}})}\left(\frac{C_{yy}}{R_y}\right), \qquad (3.5)$$

where we have chosen: x axis $||[100]$ and y axis $||[010]$. In Eqs. (3.1) and (3.2), $\mathcal{B}_1$(Ho) and $\mathcal{B}_2$(Tm) are a complex combination of the elastic constants and volume and tetragonal MEL stress contributions of the Ho and Tm layers, respectively, and they should appear in Eq. (3.1).[11] h_{subs} and C_{ij} are the thickness and quantities related to the compliance constants[19] of the substrate, respectively.

The subtraction of Eq. (3.2) from Eq. (3.3) allows the obtainment of the following relation:

$$\frac{[t_{\mathrm{Ho}}B^{\gamma,2}(\mathrm{Ho})+t_{\mathrm{Tm}}B^{\gamma,2}(\mathrm{Tm})\langle\sin^2\gamma\rangle]}{t_{\mathrm{Ho}}+t_{\mathrm{Tm}}} = 2[\sigma([010],[010])-\sigma([010],[100])]. \qquad (3.6)$$

Notice that Eq. (3.6) becomes the one used for RE SL's when the spacer layers are nonmagnetic, i.e., $B=$ Y or Lu,[8,11] and therefore Eq. (3.6) generalizes to the magnetic/magnetic SL's. We should stress that in the obtainment of Eq. (3.6) we have assumed that the magnetostriction strain $\epsilon_2^{\gamma}=\epsilon_{xy}$ is uniform for the bilayer, i.e., $\epsilon_2^{\gamma}(\mathrm{Ho})=\epsilon_2^{\gamma}(\mathrm{Tm})$, as one would expect physically. Therefore we eventually obtain different MEL stresses in the Ho and Tm layers, i.e., $B^{\gamma,2}(\mathrm{Ho}) \neq B^{\gamma,2}(\mathrm{Tm})$, for the SL equilibrium state. This distinction is important in order to understand the MEL behavior of Ho/Tm SL's or any others formed by two magnetic layers in the bilayer.

IV. ANALYSIS AND DISCUSSION OF MAGNETIZATION AND MEL STRESS MEASUREMENTS

A. Magnetic phase diagrams

The MPD of Ho/Tm and Ho/Lu SL's have been obtained from ZFC susceptibility, magnetization, and MEL stress measurements. The transition fields and temperatures were determined by the changes in the slope and or, steplike variations in the isotherm and isofield curves. By crossed tabulation of the transition temperatures at a given magnetic field, and the transition fields at a given temperature, we have obtained the H-T diagrams of the magnetic phases in the SL's of Ho/Tm and Ho/Lu, which will be compared. We have found an excellent agreement between the transition fields and temperatures obtained from the magnetization and MEL-stress isotherms. The low-field transitions were deduced from the ZFC susceptibility measurements. They are in good correspondence with the magnetic-phase boundaries determined from the neutron-diffraction experiments in Ho/Lu (Ref. 12) and Ho/Tm (Ref. 13) SL's. Figures 5(a) and 5(b) show the phase diagrams for the Ho_{30}/Lu_{15} and Ho_{30}/Tm_{16} samples, respectively. The magnetic phases of Ho_8/Tm_{16} and Ho_8/Lu_{15} are similar to the corresponding ones for Ho_{30}/Lu_{15} and Ho_{30}/Tm_{16}, although there are differences, especially at low temperatures and low fields, which have been reported[12,13] from neutron diffraction at zero field. The magnetic phases existing at high fields, $H>0.5$ T, in Ho/Lu and Ho/Tm SL's are identified by the comparison of our experimental results with the corresponding structures for bulk metals.

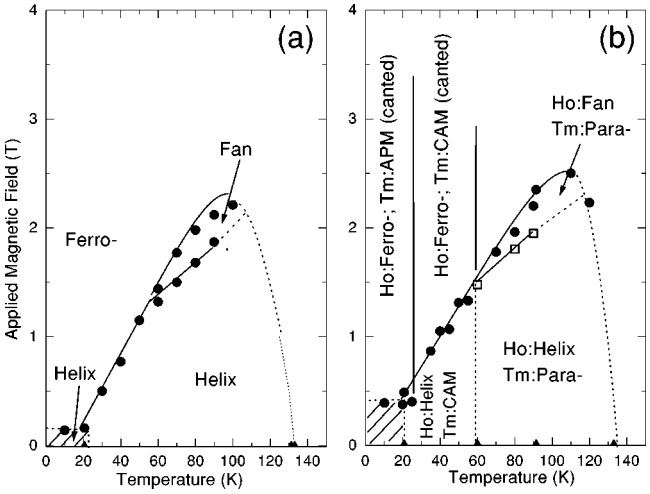

FIG. 5. Magnetic phase diagram for (a) Ho_{30}/Lu_{15} and (b) Ho_{30}/Tm_{16} superlattices. The magnetic phases shown in plot (a) are associated with the magnetic structures in holmium layers only, (●) represents the transition boundary between the helix or fan phases to a ferromagnet in holmium layers, (■) is associated with the transition boundary between the helix to fan phases in holmium layers as well. (▲) shows the transition boundary observed at low field using the ZFC susceptibility results. The dotted lines separate the different magnetic phases, which could not be detected from the experimental results and were deduced from the bulk result. APM and CPM, respectively, mean antiphase modulated and c-axis modulated structures of the thulium layers, which are canted from the c axis. The shade phase is a helix phase in holmium layers.

The "finite-size" effect, for the ferromagnetism appearance in the thin slabs of Ho,[20] was identified in Ho_8/Lu_{15} SL by neutron diffraction,[12] and is consistent with our results of ZFC susceptibility [Fig. 1(a)]. Below ~ 53 K in Ho_8/Lu_{15}, the Ho blocks behave ferromagnetically, and are coupled antiferromagnetically by the exchange, although this coupling should depend on the thickness of Lu spacer. However, in the SL of Ho_8/Tm_{16} this situation does not exist because the Tm layers destroy the finite-size effect.[13] On the other hand, there is an important reduction in the ZFC susceptibility of Ho_8/Tm_{16}, just above T_N(Tm) [see Fig. 1(c)], which is not observed in Ho_8/Lu_{15}. Above T_N(Tm), the Tm layers behave as Curie paramagnets, and the helical structure in the layers of Ho remains coherent through the Tm spacer.[13] Near T_N(Tm), there should exist strong critical fluctuations of the Tm spin-density wave, which can produce a partial disruption on the Ho helix structure, reducing the magnetic coherence of the Ho structures through the Tm spacers. This explains the above-mentioned reduction of the ZFC susceptibility. In fact, the magnetic-coherence length of the helix in the layers of Ho for Ho_8/Lu_{15} is larger than for the case of Ho_8/Tm_{16} SL.[12,13] Concerning the variation of the T_N(Ho) with regard to the bulk one, and if we assume that the T_N(Ho) is only a function of the c axis strain, only a

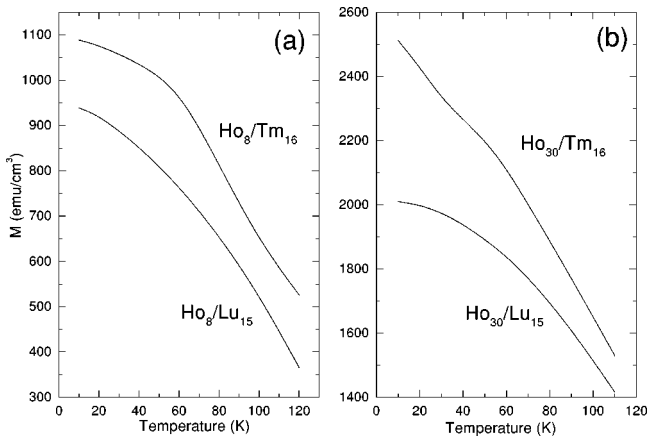

FIG. 6. Thermal variation of the magnetization at the maximum applied field of 12 T along the *b* axis for (a) Ho_8/Lu_{15} and Ho_8/Tm_{16} and (b) for Ho_{30}/Lu_{15} and Ho_{30}/Tm_{16}. Notice the smaller values for the Ho/Lu SL's, although they are fully saturated at low temperatures [see Figs. 2(a) and 2(b)].

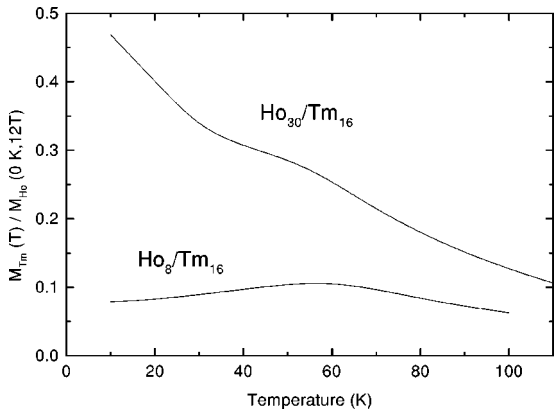

FIG. 7. Thermal dependence of the ratio between the magnetization of thulium layers in Ho_8/Tm_{16} and Ho_{30}/Tm_{16} superlattices and the saturation magnetization of holmium layers in the isomorphous Ho/Lu SL's, at the maximum field of 12 T, applied along the *b* axis.

variation of 4 K can be explained,[12,13,22] whereas reductions of 15 K in the case of Ho_8/Lu_{15} and of 25 K in Ho_8/Tm_{16} are observed [see Figs. 1(a) and 1(c)]. So, the changes of T_N(Ho) must be mainly correlated with the dilution degree of these systems.

There exist some enhancements of the transition fields from helix to ferromagnetic or to fan phases in the interleaving holmium layers in the Ho/Lu and Ho/Tm SL's. In fact, in Fig. 5 we may appreciate that the differences of the transition fields of Ho/Lu and Ho/Tm SL's are not larger than 0.5 T. We argue that the reason for this small enhancement is due to the stability of the helix structure in the Ho layers, against the applied magnetic-field distortion. The epitaxial strain can be one of the reasons for the enhancement, because the *c* axis exchange interaction should be modified by the misfit strain. On the other side, there exists another possible factor that could explain this enhancement. It has been argued that in Ho/Y SL's, the enhancement is mainly due to the existence of the yttrium spacer.[23] The extraordinary peak calculated in the generalized susceptibility of the conduction-band electrons in yttrium[24] can enhance the Ruderman-Kittel-Kasuya-Yosida (RKKY) exchange $f-f$ between holmium ions in holmium-yttrium SL's. In our case, we could have the same situation, but now the eventual enhancement in the exchange coupling is introduced by the thulium spacers, because the exchange values in Tm bulk are larger than in Ho bulk.[21]

B. High-field magnetization

In Figs. 6(a) and 6(b) we have represented the thermal dependence of the magnetization values at the maximum magnetic field applied, 12 T, for Ho/Lu and Ho/Tm SL's. We observe that the magnetization values for Ho/Tm SL's are much larger than the corresponding ones of Ho/Lu SL's. In the Ho/Lu case, the values at low temperatures are close to the full saturation expected from the bulk values. For Ho/Tm SL's, we argue that at high-field only the Ho layers are fully saturated along the applied field direction as it happens for the Ho/Lu case, but in Tm layers a strong anisotropy exists along the *c* axis, so the 12 T magnetic field along the *b* axis is not enough to saturate the Tm layers. To ascertain the magnetization behavior in Tm layers, we have proceeded to subtract the Ho contribution from the total magnetization in both Ho/Tm SL's. We have assumed that in the Ho/Tm SL's the Ho magnetization is the same as in the Ho/Lu SL's. The Ho_8/Tm_{16} and Ho_{30}/Tm_{16} SL's behave very differently (see Fig. 7). Notice that, in the zero temperature limit, for the first SL the Tm basal-plane magnetization is less than 10% of the Ho one, while for the latter, it is nearly half of it. The Tm magnetization M_{Tm} shows a peak at about 58 K for Ho_8/Tm_{16} SL, which is precisely the Néel temperature of Tm layers. Below 58 K, M_{Tm} smoothly decreases with temperature. This thermal behavior of M_{Tm} (12 T) is similar to that observed in bulk Tm, when the magnetic field is applied along the *b* axis.[6] The situation is completely different in Ho_{30}/Tm_{16} SL: M_{Tm} (T, 12 T) only shows a shoulder at about 58 K, and increases continuously on decreasing the temperature. This increase points to a stronger exchange coupling between the Ho and Tm layers in this SL, which is consistent with zero-field neutron-diffraction results.[13]

The above results indicate that, for Ho_8/Tm_{16}, the tilting of the M_{Tm} out of the *c* axis comes mainly from the torque exerted by the external applied magnetic field, although some exchange with the Ho layers exists, while in the Ho_{30}/Tm_{16} SL the stronger contribution to the mean field acting on the Tm ions supplied by the Ho layers is clearly shown up.

C. Magnetoelasticity in the basal plane of Ho/Lu and Ho/Tm SL's

In this section, we proceed to a comparative analysis of the MEL behavior within the basal plane for Ho/Tm and Ho/Lu SL's at the maximum field applied of 12 T. In Figs. 8(a) and 8(b), we show the basal-plane CSB effective MEL stress values, $2\{\sigma([010],[010])-\sigma([010],[100])\}$, for Ho_8/Lu_{15} and Ho_8/Tm_{16} and for Ho_{30}/Lu_{15} and Ho_{30}/Tm_{16}

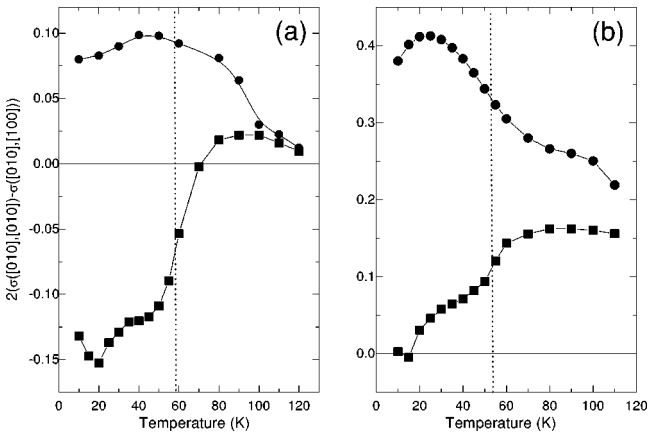

FIG. 8. Thermal variation of the measured magnetoelastic stress within the basal plane for (a) Ho_8/Lu_{15} (●) and Ho_8/Tm_{16} (■) superlattices, and (b) for Ho_{30}/Lu_{15} (●) and Ho_{30}/Tm_{16} (■) superlattices, at the maximum field of 12 T applied along the *b* axis. The continuous line represents only a visual guide. The dotted line separates the paramagnetic and magnetically ordered phases for thulium layers.

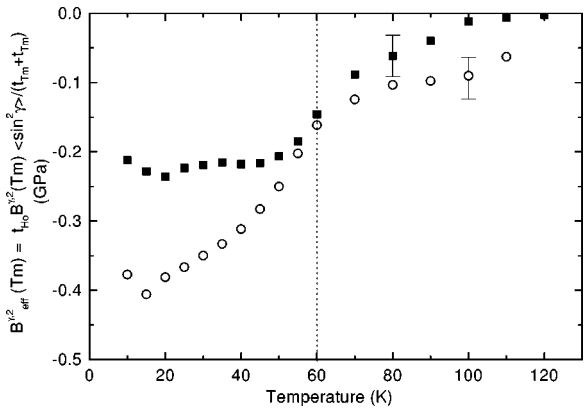

FIG. 9. Thermal variation of the magnetoelastic stress of thulium layers within the basal plane for Ho_8/Tm_{16} (■), and Ho_{30}/Tm_{16} (○), at the maximum applied field of 12 T. The dotted line separates the temperature above which the thulium layers show parastriction.

SL's against temperature, respectively. At high temperatures (≈ 100 K), the CSB effective MEL stress for both SL's have close values, as is expected because the MEL stress behavior is dominated by the Ho layers. However, on decreasing the temperature, the $2(\sigma([010],[010])-\sigma([010],[100]))$ MEL stress in Ho/Tm SL's deviates from the Ho/Lu values. In spite of this deviation is larger in Ho_{30}/Tm_{16} than in Ho_8/Tm_{16}, for the latter SL there exists an important qualitative difference, which is the sign change of the MEL stress at around 70 K. We can explain this sign change if we consider that the MEL stress in the basal plane is of single-ion crystal electric-field (CEF) origin,[14,15] and proportional to Stevens factors α_J, which are of the same order and *opposite* sign for both Ho^{3+} and Tm^{3+} ions. So, in Ho_8/Tm_{16}, because of its relative volume, the Tm can produce a sign change in the CSB MEL stress parameter, whereas in the Ho_{30}/Tm_{16} can only decrease the value of MEL stress, especially below T_N (Tm) [see Fig. 8(b)].

The MEL behavior of the Ho blocks in Ho/Tm SL's can be reasonably assumed to be close to that one in Ho/Lu SL's.[8,11] In Sec. IV B, we argued that the magnetization of Ho layers is fully saturated along the field direction for the high-field regime, $H>5$ T; however, for the Tm ones it is hardly tilted towards the field, even at 12 T. Now, we keep the same assumption for the MEL stress associated with the Ho layers. So, by using Eq. (3.6) and the values displayed in Figs. 8(a) and 8(b), we have obtained the effective MEL stress $B^{\gamma,2}_{eff}$(Tm) at 12 T, associated with the CSB in Tm blocks (see Fig. 9). These results, at low temperatures, seem to be consistent with those obtained from magnetization, i.e., the Tm ions are more polarized along the *b* direction in the case of Ho_{30}/Tm_{16} SL than in the Ho_8/Tm_{16}. The origin of such tilting should be associated to the magnetic coupling between the Ho and Tm ions through the interface, as the neutron diffraction suggests at zero field.[13] On the other hand, $B^{\gamma,2}_{eff}$(Tm) values scale roughly with the square of the magnetization of Tm ions, M^2_{Tm}, for temperatures above T_N(Tm), as expected.[14,15] In Fig. 9 are represented the MEL values of Tm layers, which are negative, as expected for Tm ions, and different from each other, which could indicate the existence of epitaxial and interfacial contributions, as previous studies showed in other RE SL's.[7,11]

V. CONCLUSIONS

We have studied the magnetic and basal-plane magnetoelastic behavior for Ho_8/Tm_{16} and Ho_{30}/Tm_{16} SL's. We have measured the low-field and the high-field magnetization applying the magnetic field along the *hexagonal b axis*, between 10 and 120 K. The zero-field-cooled magnetization clearly shows the coexistence of Ho and Tm magnetic ordering below T_N^{Tm}, although the Ho blocks are magnetically ordered below 100 K in both SL's. The analysis of the high-field magnetization (at 12 T) shows that the Ho magnetic moments are fully aligned along the field direction above 5 T for both Ho/Tm SL's, and that the Tm layers behave similarly to bulk Tm only for Ho_8/Tm_{16}. For Ho_{30}/Tm_{16}, the low-temperature values of magnetization indicate a larger tilting of the Tm magnetic moments out of the *c* axis with respect to the bulk one. The analysis of the MEL stress experiments also indicate that the Tm moments are tilted out from the *c* axis when a magnetic field is applied within the basal plane of the hcp structure (otherwise the values of $B^{\gamma,2}$ would be nearly the same as for the Ho/Lu SL's), this effect being larger in the case of the Ho_{30}/Tm_{16} sample than for the Ho_8/Tm_{16} SL. Nevertheless, experiments in higher magnetic fields would be necessary to attempt the full saturation of these competing anisotropy SL's, and, in this way, to be able to obtain separately the Tm and Ho MEL stress parameters. The different tilting of Tm ions in the two studied Ho/Tm SL's can be due to differences in the mean field originated by the Ho layers (strongest in the Ho_{30}/Tm_{16} SL), which can

give rise to different couplings between the Tm bilayers (as shown by the neutron-diffraction experiments[13]). Also, a different effect of the basal-plane CSB MEL strain, ϵ_1^γ, in Tm layers in both SL's, could cause unlike changes of the B_2^0 and B_6^0 CEF parameters and, consequently, unlike modifications of the axial anisotropy of Tm blocks (weakest for the Ho_{30}/Tm_{16} SL).

ACKNOWLEDGMENTS

We are grateful to the Spanish CICYT for the supporting grants MAT97-1038, MAT99-1063-C04-01, and MAT2000-1290-C03-01. L.B. acknowledges the Ph.D. grant from the Spanish Foundation ''Ramón Areces.'' We are grateful to Professor R. A. Cowley and Dr. P. A. J. de Groot for early discussions about this work.

[1] W.C. Koehler, J.W. Cable, E.O. Wollan, and M.K. Wilkinson, J. Appl. Phys. **33**, 1124 (1962).
[2] W.C. Koheler, J. Appl. Phys. **36**, 1078 (1965).
[3] W.C. Koehler, J.W. Cable, M.K. Wilkinson, and E.O. Wollan, Phys. Rev. **151**, 414 (1966).
[4] W.C. Koehler, J.W. Cable, M.K. Wilkinson, and E.O. Wollan, Phys. Rev. **158**, 450 (1967).
[5] J.L. Feron, Ph.D. thesis, University of Grenoble, 1969.
[6] D.B. Richards and S. Legvold, Phys. Rev. **186**, 508 (1969).
[7] M. Ciria, J.I. Arnaudas, A. del Moral, G.J. Tomka, C. de la Fuente, P.A.J. de Groot, M.R. Wells, and R.C.C. Ward, Phys. Rev. Lett. **75**, 1634 (1995).
[8] M. Ciria, Ph.D. thesis, University of Zaragoza, 1997.
[9] A. del Moral, M. Ciria, J.I. Arnaudas, M.R. Wells, R.C.C. Ward, and C. de la Fuente, J. Phys.: Condens. Matter **10**, L139 (1998).
[10] A. del Moral, M. Ciria, J.I. Arnaudas, and C. de la Fuente, Phys. Rev. B **57**, R9471 (1998).
[11] J.I. Arnaudas, A. del Moral, M. Ciria, C. de la Fuente, R.C.C. Ward, and M.R. Wells, in *Frontiers in Magnetism of Reduced Dimension Systems*, Vol. 49 of *NATO Advanced Study Institute, Series B: Physics*, edited by V.G. Baryakhtar, P.E. Wigen, and N.A. Lesnik (Kluwer Academic Publishers, Dordrecht, 1998), p. 525.
[12] P.P. Swaddling, D.F. McMorrow, J.A. Simpson, M.R. Wells, R.C.C. Ward, and K.N. Klausen, J. Phys.: Condens. Matter **59**, L481 (1993).
[13] R.A. Cowley, J.A. Simpson, R.C.C. Ward, M.R. Wells, and D.F. McMorrow, J. Phys.: Condens. Matter **10**, 2115 (1998).
[14] E.R. Callen and H.B. Callen, Phys. Rev. **139**, A455 (1965).
[15] E.J. Callen, J. Appl. Phys. **53**, 8139 (1982).
[16] R.C.C. Ward, M.R. Wells, C. Bryn-Jacobsen, R.A. Cowley, D.F. McMorrow, and J.A. Simpson, Thin Solid Films **275**, 137 (1996).
[17] R.C.C. Ward and M.R. Wells (private communication).
[18] *Theory of Plates and Shells*, edited by S. Timoshenko and S. Woinowsky-Kriger (McGraw-Hill, New York, 1959), Vol. 2.
[19] W.E. Tefft, J. Res. Natl. Bur. Stand., Sect. A **70A**-403, No. 4, 277 (1966).
[20] J. Bohr, Doon Gibbs, J.D. Axe, D.E. Moncton, K.L. D'Amico, C.F. Majkrzak, J. Kwo, H. Hong, C.L. Chien, and J. Jensen, Physica B **159**, 93 (1989).
[21] K.A. McEwen, U. Steigenberger, and J. Jensen, Phys. Rev. B **43**, 3298 (1991).
[22] H. Umebayashi, G. Shirane, B.C. Frazer, and W.B. Daniels, Phys. Rev. **165**, 688 (1968).
[23] C. de la Fuente, R.A. Cowley, J.P. Goff, R.C.C. Ward, M.R. Wells, and D.F. McMorrow, J. Phys.: Condens. Matter **13**, L141 (1999).
[24] S.H. Liu, R.P. Gupta, and S.K. Sinha, Phys. Rev. B **4**, 1100 (1971).